

# Improving Accuracy of Powder Sintering-based SFF Processes by Metal Deposition from Nanoparticle Dispersion

N. B. Crane<sup>\*</sup>, J. Wilkes<sup>†</sup>, E. Sachs<sup>†</sup>, S. M. Allen<sup>‡</sup>

Reviewed, accepted August 26, 2005

<sup>\*</sup> Sandia National Laboratories, PO Box 5800 MS 0958, Albuquerque, NM 87185-0958

<sup>†</sup> Department of Mechanical Engineering, MIT, 77 Massachusetts Ave, Cambridge, MA 02139

<sup>‡</sup> Department of Materials Science and Engineering, MIT, 77 Massachusetts Ave, Cambridge, MA 02139

## ABSTRACT

Solid Freeform Fabrication processes such as three-dimensional printing (3DP) and selective laser sintering (SLS) produce porous parts that must be densified. New steel infiltration methods can produce parts of standard alloy compositions with properties comparable to wrought materials. However, the infiltration process introduces dimensional errors due to both shrinkage and creep—particularly at the high temperatures required for steel infiltration. A post-processing method has been developed to reduce creep and shrinkage of porous metal skeletons. Tests have achieved over 90% reduction in creep and 50% reduction in shrinkage. In this method, metal is deposited into the porous part from a suspension of metallic nanoparticles. These particles densify at low temperatures to reinforce the bonds and reduce stress concentrations that amplify creep deformation in untreated parts. After treatment, the reinforced parts can be densified by infiltration.

## INTRODUCTION

Solid freeform fabrication (SFF) processes offer great geometrical flexibility in manufacturing while eliminating the time and expense of part specific tooling. These advantages make them very attractive for creating appearance models and prototypes and for direct production in low volumes [1]. However, direct part production requires much greater process capability than appearance models and prototypes. This work addresses the dimensional accuracy limitations of parts prepared by Three-Dimensional Printing (3DP) and Selective Laser Sintering (SLS) so that they might be more suitable for applications demanding high accuracy and good properties. Both 3DP and SLS produce parts at high rates by binding powder together, typically with a polymer [2,3]. After forming the geometry, the parts consist of ~50–100  $\mu\text{m}$  particles bound together.

For prototype and production applications, the material properties are improved by sintering the powder to full density or infiltration with a second material. Typically, large metal parts are produced in steel powder that is infiltrated with bronze with a linear shrinkage of ~1–3% [4,5]. The resulting bronze-steel composite is inferior to homogenous steel alloys and is not widely accepted by designers. New infiltration methods can produce homogenous final parts of standard ferrous alloys [6,7]. Homogenous steel infiltration produced parts with composition and properties comparable to wrought D2 tool steel (1.5% C, 12% Cr, 1% V, 1% Mo, Bal Fe).

At liquid-metal infiltration temperatures, sintering and creep processes are active. Both can reduce the final dimensional accuracy. The increase in infiltration temperatures moving from

bronze to steel infiltration substantially increases shrinkage and creep deformations during infiltration, reducing the dimensional accuracy.

Typically parts are supported by refractory powder during infiltration to reduce creep deflections. However, many shapes are difficult to pack consistently, and inconsistent packing can increase variation in the final geometry. Additionally, shrinkage differences between the supporting powder and the parts can tear or deform the part during sintering and infiltration.

This work describes and demonstrates a nanoparticle binder and treatment method that can dramatically reduce the deflection rates and shrinkage during infiltration so that the final part accuracy is improved. Section 2 will describe this technique. Section 3 describes the test methods used to evaluate the benefits of the technique. Section 4 discusses the improvements in dimensional accuracy that were achieved and the conditions for optimal performance. Section 5 considers the mechanisms by which the improvements were obtained.

## PROPOSED NANOBINDER

Sintering shrinkage and creep deformation under self-weight both cause dimensional changes during infiltration. The rate of shrinkage and creep are both strongly dependent on the size of the bonds between the micron-scale skeleton particles. While sintering can increase these bond sizes, the shrinkage is increased and the parts may still creep during sintering. Alternatively, if the bond size is increased from added material, both creep and shrinkage can be decreased. [8]

We have used a dispersion of metal nanoparticles to increase the size of the necks between particles and thus reduce the dimensional changes during post-processing. This dispersion could be added either by direct inkjet printing in 3DP or it could be infiltrated into parts produced by 3DP or SLS, powder injection molding, or other processes after the geometry is formed. The dispersed nanoparticles can easily fit through the pores between the  $\sim 75 \mu\text{m}$  particles to reach the particle bonds.

After applying the dispersion to the skeleton particles, the solvent can be evaporated to deposit the particles in the skeleton. The solvent dries last from the high curvature areas such as the contacts between particles, concentrating the nanoparticles in these regions. On heating, these particles will sinter to enlarge the neck size and reduce the stress in the bonds. As nanoparticles sinter at much lower temperature than micron-scale particles [9,10], the nanoparticles can densify while the surrounding skeleton powder sinters very little if any.

In the special case of ferromagnetic nanoparticles deposited into skeletons of ferromagnetic materials, the nanoparticles can be concentrated in the contact locations even more effectively by applying a DC magnetic field during drying. When a magnetic field is applied along the skeleton, there is a gradient in the field at the contacts between the micron-scale particles that draws the nanoparticles into these regions.

The particles in the dispersion can be chosen to be compatible with the composition of the final part so that the final material properties are not degraded. In steel parts, iron particles are ideal as adding several percent more iron will have a very small impact on the total part composition. Alternatively, a material with a lower creep rate could be chosen that might create bonds with a higher creep resistance, but the impact on the final part properties must be considered. Any

composition gradients created will exist over a few microns and will be reduced by diffusion at high temperatures.

This nanoparticle binder process was tested using a gas-atomized, spherical 410 SS (12 Cr, 0.15 C, Balance Fe) skeleton powder sieved to 63–90  $\mu\text{m}$  size. The nanoparticle dispersion was a commercial product called NanoIron produced by NanoMat. It consists of monodisperse iron nanoparticles with an average size between 7–10 nm. The solvent is a proprietary organic solvent with a boiling point of 287°C. The typical concentration of the nanoparticles was 0.5 vol%.

## EXPERIMENTAL METHODS

The nanobinder process was tested using a simple test bar with an unsupported overhang as illustrated in **Figure 1**. These bars were produced either by 3DP using a traditional polymer binder or by sintering powder in an alumina mold. In both cases they were sintered to 1000°C for 30 minutes to develop handling strength and decompose the polymer binder used in the 3D printed parts.



**Figure 1** Schematic representation of a deflection test bar in an unsupported position (left) and supported position (right).

The nanoiron was applied to the bars by infiltration at room temperature. The solvent was dried at 150°C and the nanoparticles sintered at 700°C for 10 minutes. In most bars, the application process was then repeated to increase the quantity of deposited iron. The drying was done in a nitrogen atmosphere and the sintering in forming gas (95% Ar, 5% H<sub>2</sub>) to minimize oxidation of the nanoparticles. After applying the nanoiron, some bars were “presintered” by heating them in a supported position (upside down) to 1100°C or 1300°C and holding 60 minutes. The creep strength of the bars was tested by heating in an unsupported position to 1284°C and measuring the final deflection of the tip.

The creep and shrinkage performance of the specimens was measured by heating both nanobinder treated and untreated specimens through the same heat cycle and comparing the creep deflections of the tip. The tip deflections were measured using either an optical comparator or images from a flat bed scanner. The length of the supported section was also measured using an optical comparator to calculate linear sintering shrinkage. The ratio of tip deflection of treated specimens to untreated control specimens was used to compare the relative benefit achieved under different treatment conditions. Smaller values of the deflection ratio indicate more benefit from the nanobinder treatment.

To better understand the performance of the process, the drying rate, oxidation state of the nanoparticles, and number of nanobinder applications were varied. The drying rates consisted of fast (hold 20 minutes at 150°C and heat to 300°C in 20 minutes, 1–2 scfh gas flow), moderate (hold 20 minutes at 150°C and heat to 300°C in 200 minutes, 1–2 scfh gas flow) and slow (hold 24 hours at 150°C and heat to 300°C over 4 hours, <0.1 scfh gas flow).

The effect of the oxidation state was compared by applying the same amount of nanoiron from the same batch to two skeletons. One portion of the nanoiron was allowed to oxidize in open air for several days before application while the second was maintained in an inert atmosphere. The two bars were deflected at the infiltration temperature.

Some bars were placed in a reservoir of nanobinder during drying so that as the solvent evaporated, additional binder would infiltrate into the skeleton. Using this method, larger quantities of nanobinder could be deposited in a single application and the creep rates could be compared to samples with the same amount of nanobinder added but in multiple applications. The nanoparticles shrink during sintering, potentially breaking the bonds formed between the particles. However, a repeated application of the nanobinder would partially fill the voids.

Some samples were also dried under a magnetic field to improve the concentration of nanoparticles at the contact points between particles. A magnetic field was applied along the length of the bar by placing a rare earth magnet at each end of the specimen during the drying phase. The magnets were removed after the 150°C drying phase to avoid heating above their Curie temperature.

## RESULTS

The nanobinder reduced both the creep deflection (deflection ratio < 1) and the shrinkage. The quantity of the nanobinder added, oxidation state, drying rate, and applied magnetic fields each had a significant impact on the nanobinder performance. The best results were obtained by using unoxidized suspensions dried under a magnetic field, with multiple applications. When drying without a magnetic field, better results were achieved by drying at faster rates. In the best case, nanoiron treatment reduced the deflection by 95% as illustrated in **Figure 2**. The sintering shrinkage of this specimen was also reduced by 60%. This was achieved by applying 2.7 wt% nanoiron in four application cycles dried under a magnetic field. The effect of each of these variables is discussed below.



**Figure 2 Photo comparing the deflection of 410 stainless steel bars with and without nanoiron treatment.** The treated bar received four applications and was dried under a magnetic field. Both bars were deflected without prior sintering except the 1000°C sintering required to create the initial geometry.

## DISCUSSION OF RESULTS

### Drying Rate

**Figure 3** compares the deflection ratios of bars dried under different conditions as a function of the quantity of nanobinder added to the skeletons. In general, the tip deflection decreases with increasing nanobinder deposition as would be expected. However, greater benefit is obtained at moderate and quick drying rates than at slow drying rates. This is due to changes in the distribution of the nanoiron deposits with drying speed. At higher drying rates, the deposits are concentrated at the outside of the skeleton where the bending stresses are highest. Thus, greater improvement is obtained than if the deposit were distributed more uniformly. The deposit distribution was observed by drying nanoiron in porous cylindrical copper specimens at fast, moderate, and slow drying rates. The parts were sectioned, and EDX spectroscopy was used to measure the relative iron deposit level as a function of distance from the free drying surface. The EDX measurements were made sampling the entire field of view in the SEM at a magnification of 500X. **Figure 4** shows that the faster drying rates deposit more material at the outer edge. Even at slow drying rates, the concentration is somewhat higher at the exterior. Previous studies [11,12] have shown that the drying conditions can be adjusted to concentrate the deposits on the interior or exterior or uniformly throughout.

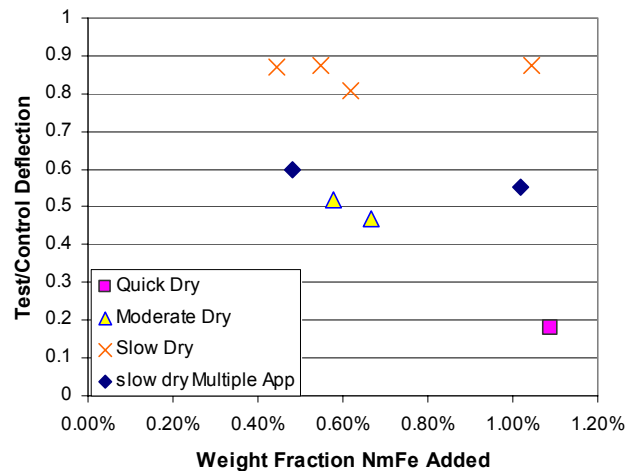


**Figure 3 Summary of deflection data as a function of drying conditions and quantity of binder material added to the part.** Deflection decreases with faster drying rates, increased number of applications, and increasing quantity of deposited material.

### Multiple Binder Applications

On heating the nanoparticle deposits, they sinter and shrink. The shrinkage can break the bonds between particles as seen in **Figure 5**. However, if the nanobinder is reapplied the cracks can be repaired and on heating, any new cracks will be smaller than before as illustrated. Indeed, when varying amounts of nanoiron were added in a single application, the deflection ratio was approximately 0.85 and did not decrease at larger quantities. However, when the nanoiron was applied in multiple applications, the deflection ratio decreased and showed increasing benefit with increasing deposit volume as shown in **Figure 6**.

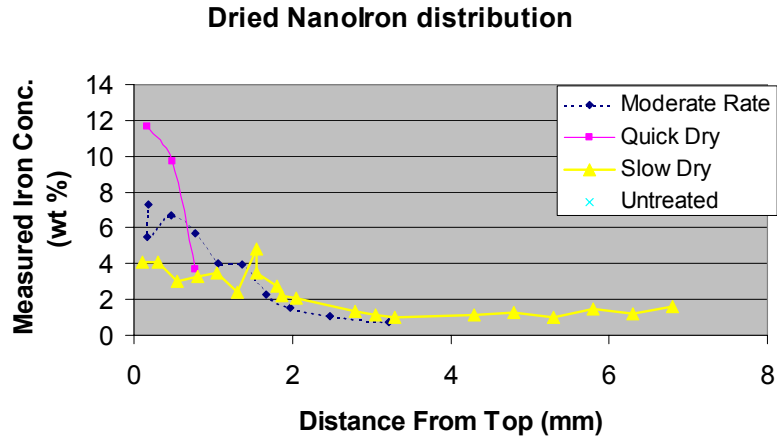


**Figure 4 Distribution of iron deposits in copper plugs for various drying conditions.** Concentration measurements made using EDS across the whole field of view at a magnification of 500X down the centerline of a cylinder of sintered copper powder. The faster drying rates concentrate more material in a thinner region on the outside of the sample. Since the bending stresses are highest on the outside, the effectiveness of the nanobinder increases.

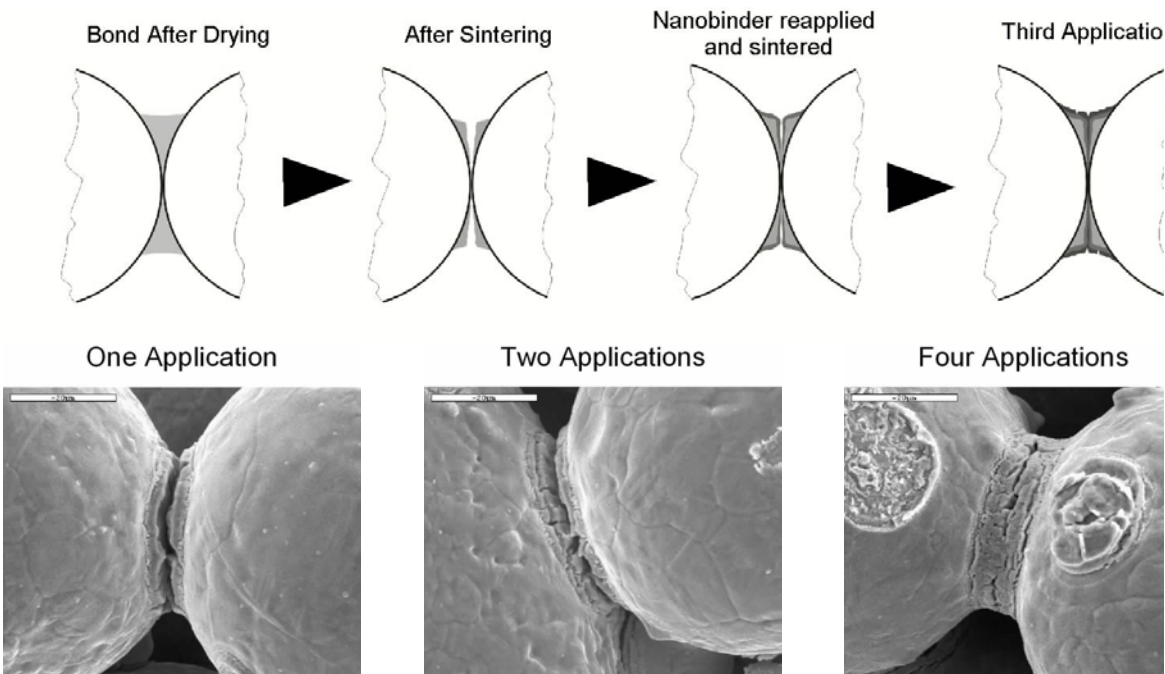


**Figure 5 Applying the nanobinder multiple times both enlarges the bonds and heals cracks formed by sintering shrinkage. (Top)** Schematic illustration of bond repair by multiple applications of nanobinder. **(Bottom)** Images comparing bonds sintered to 700°C in samples with 1, 2, and 4 applications and dried under a magnetic field. The size of the cracks in the bonds decreases with additional applications.

## Drying in a Magnetic Field

Drying under a DC magnetic field dramatically reduces the deflection ratio compared to samples dried without a magnetic field at a moderate rate as seen in **Figure 6**. SEM images of broken interparticle bonds show that the bonds are much larger when dried under a magnetic field than without. This suggests that without the magnetic field, many of the nanoparticles are deposited on the surface of the micron-scale skeleton particles where they do not directly reduce the shrinkage rate.

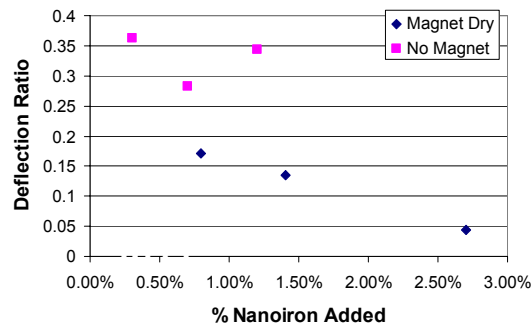


**Figure 6 Deflection ratios for nanoiron specimens dried with and without a magnetic field.** Samples dried under a magnetic field have lower deflections than comparable samples dried without a magnetic field. Data includes samples that were presintered at 1300°C and samples deflected directly after processing the nanoiron.

## Oxidation of the Nanoparticles

The oxidized nanoparticles reduced the creep deflection by 48%, but the same weight of unoxidized material reduces the creep deflection by 64% relative to the untreated case. This difference could be the result of changes in the volume and carbon content of the deposits with oxidation. Iron oxide crystals contain approximately half the iron per unit volume of metallic iron. When the iron oxide is reduced to iron on heating, the deposit density is reduced and the sintering shrinkage for densification increases. Thus, the bonds are more likely to break and more applications of the nanobinder may be required to heal them.

The oxides are reduced to iron when the nanoiron deposits are heated, even in an inert atmosphere. Thus, the oxide must be reduced by the carbon residues of the ligands that stabilize the nanoparticles in the suspension. The carbon-oxygen reaction substantially reduces the carbon content in the skeletons as seen by the difference in carbon content between oxidized and unoxidized nanoiron deposits after heating. Oxidized and unoxidized nanoiron deposits were both heated to 700°C in forming gas and the carbon content of each was measured by combustion infrared detection. The oxidized suspension contained less than 1% carbon compared to 9.7% for unoxidized suspensions under the same conditions. As discussed below, the carbon deposits seem to play an important role in decreasing the creep deflection.

Despite these limitations, the oxidized nanoparticles did significantly reduce the creep deformation of the bars. Oxidized nanoparticles are easier to work with than metallic nanoparticles due to their stability in air. Perhaps if carbon can be added to offset that which reduces the iron oxides, the oxidized particles could be effectively used in the nanobinder at lower cost than for metallic particles.

## Shrinkage Reduction from the Nanobinder

**Figure 7** shows that the nanobinder consistently reduced the sintering shrinkage of the skeletons. The reduction varies from 40–60% with some increase in reduction with larger deposits. While the creep deflections were sensitive to drying conditions and oxidation state of the suspension, neither of these variables had a significant effect on the shrinkage. This relationship warrants further investigation.

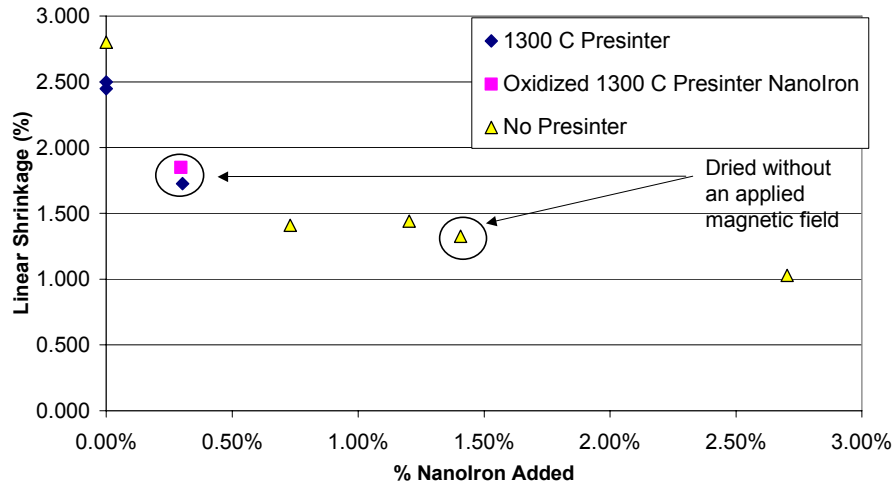


**Figure 7 Variation in shrinkage reduction with quantity of nanoiron added.** Total shrinkage reduction is approximately 50% with some increase in shrinkage reduction with increasing nanoiron quantity of deposits. There is not sufficient data to draw conclusions regarding the nature of the relationship. The oxidized nanoparticles are almost as effective at reducing the shrinkage as the unoxidized nanoparticles. Also, the application of a magnetic field during drying does not appear to change the drying shrinkage significantly.

## MECHANISMS OF CREEP REDUCTION

Additional experiments were conducted to understand the mechanisms by which the nanobinder treatment reduced the creep deformations of the test specimens. Two important mechanisms were identified: increased bond size and carbon deposition. Each is discussed below.

### Bond Size Increases

The sizes of sintering bonds in parts with and without nanobinder treatment were compared by measuring the size of broken bonds in SEM images of fracture surfaces. Of the two pairs, C-25 & C-18 were presintered at 1300°C while C-29 and C-32 were not. The treated sample in both pairs was dried under a magnetic field to concentrate the deposits in the bonds and improve the deposit uniformity. The average bond size and the number of bonds of both treated samples increased relative to the untreated samples. The difference was particularly distinct in the bars that were not presintered as illustrated in **Figure 8**.

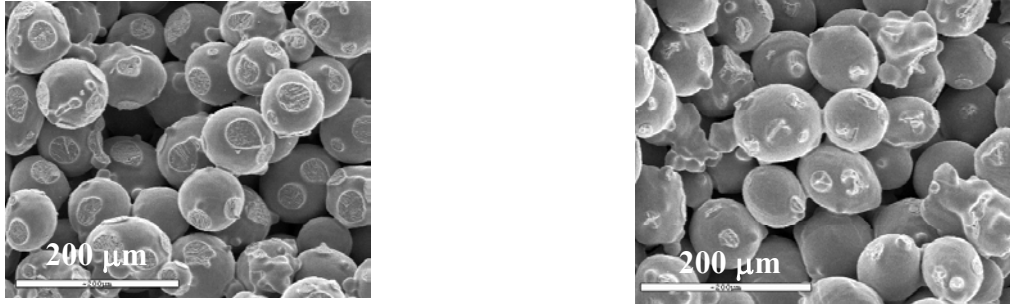


**Figure 8 Change in bond area with and without nanobinder treatment.** After heating the bars through a deflection cycle, the bars were fractured and the area of exposed bonds compared. The nanobinder treated part (**left**) has much more bond area than the untreated bar (**right**).

### Carbon Deposition

The carbon composition of dried nanoiron deposits was measured by combustion infrared detection as 9.7% carbon. While carbon can lower the activation energy for self-diffusion of iron, it also can lower the probability of a successful jump of an iron-atom due to its affinity for vacancy sites. Thus, adding carbon can directly decrease iron diffusivity in the alloy at high temperatures. [13] Adding carbon can also change the diffusivity by changing the stable phases present. The pseudo-binary phase diagram of **Figure 9** shows that adding carbon to the base 410 SS composition can shift the equilibrium out of the two-phase  $\alpha$ - $\gamma$  region, reducing the grain boundary area available for diffusion and eliminating the higher-diffusivity  $\alpha$  phase.

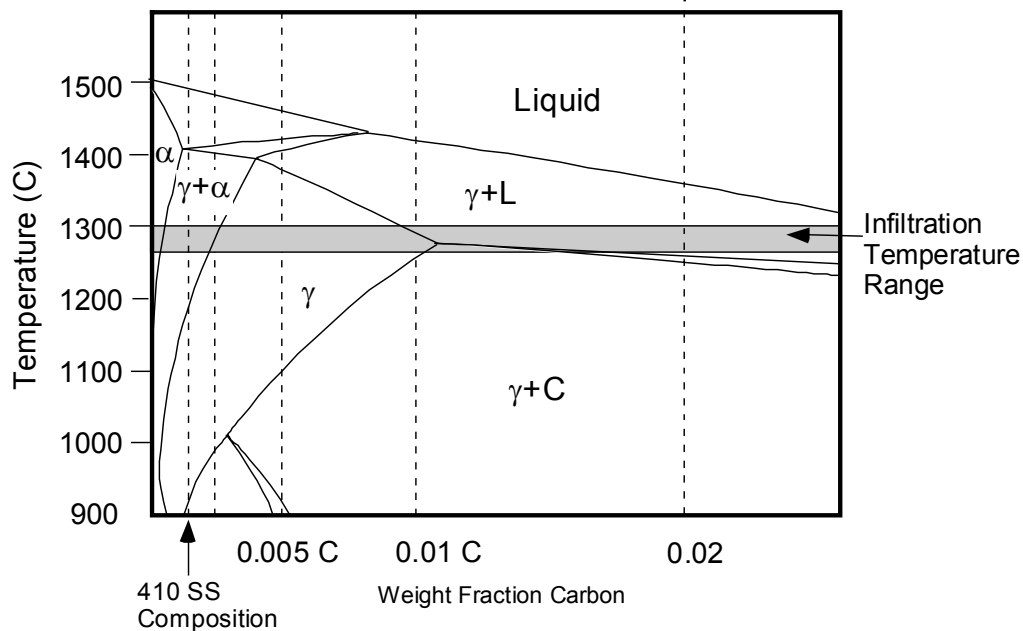


**Figure 9 Pseudobinary phase diagram for 410 SS.** The basic 410 composition with 0.16% carbon is single phase austenite ( $\gamma$ ) between approximately 950°C and 1200°C. If the carbon is increased to 0.25%, only the austenite phase is stable between 1000°C and the infiltration temperature. Diffusional creep may be lower in the single-phase region.

The effect of carbon on the deflection of the specimens was tested in two ways. First, a test specimen was infiltrated with a commercial 3DP binder obtained from ProMetal called “Binder S”. This binder leaves residual carbon on decomposition. A second specimen was molded from 420 SS (13 Cr, 0.4 C, Bal Fe) and sintered to 1000°C. Both of these specimens were deflected and compared to a molded 410 SS skeleton prepared in an alumina mold as before and deflected. The carbon content of both samples was measured by combustion infrared detection. **Figure 10** shows the deflection ratio of these specimens as a function of the carbon composition. The added carbon clearly reduces the deflection. This suggests that the carbon deposited with the nanobinder is largely responsible for the reduced creep deformation.

To test whether the added iron is important, the carbon composition of a number of nanobinder treated skeletons was measured and plotted on the same graph. Magnet-dried samples were used to assure that the deposits were uniformly distributed. These samples show that there is clearly more benefit from samples with both iron and carbon deposited rather than just carbon.

The effect of the nanobinder on the deflection performance is particularly dramatic when the samples are not sintered at 1300°C before deflection. When the presinter step was removed from the high-carbon 420 SS parts, the deflection was comparable to a 410 SS part without presinter (deflection ratio ~ 1). In contrast, the nanoiron treated parts without a presinter step still showed very large improvements relative to similarly processed 410 SS parts (small deflection ratios).

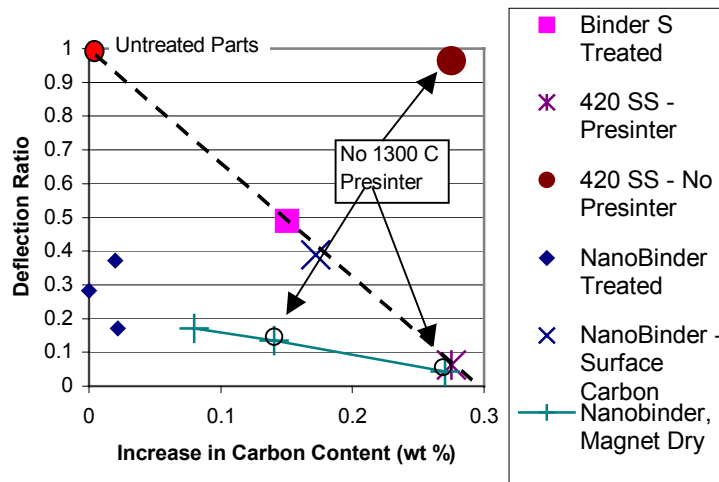


**Figure 10** Deflection ratios for treated and untreated bars plotted against the change in carbon composition of the specimen relative to the basic 410 SS composition. Samples include 420 SS material, polymer binder in 410 SS, and nanoiron treatment of 410 SS powder. The carbon treated parts show significant creep reductions, but smaller than the nanoiron treated parts. Additionally, the nanoiron parts follow similar trends with and without a presinter at 1300°C while the 420 SS bars with carbon added have very high deflection ratios (low benefit of carbon) unless it is presintered at 1300°C.

This case is particularly important in practical applications because in general it is impossible to presinter the parts at high temperature without incurring creep deformations and/or difficulties with packing the parts in supporting powder. Additionally, the extra step increases the time and cost of the post-processing. It is therefore most desirable to heat the samples for infiltration directly after nanobinder treatment. It is in this case when the iron added to the skeleton from the iron nanobinder is most valuable.

These results are consistent with the conclusion that the added carbon reduces the self-diffusion rate in the alloy. If the diffusion rate is reduced, both creep rate and sintering rate are reduced. As a result the sinter bonds are smaller when the carbon content is higher. Without the presintering step, the sintering bonds are very small. Under the high resulting stresses, they quickly fail due to high creep strain. When the bars are treated with nanoiron, the deposits: (1) increase the carbon content to reduce the creep rate and (2) enlarge the bonds between the particles so that the stress is reduced.

## CONCLUSIONS

Steel infiltration processes can produce homogenous, dense material from porous metal skeletons such as those produced by powder injection molding, 3D Printing (3DP), and Selective Laser Sintering (SLS). Despite the improved material properties possible through steel infiltration, at the high infiltration temperatures, dimensional accuracy is reduced by creep deformations under the structure self-weight and sintering shrinkage.

Iron nanoparticles have been applied to porous metal skeletons by infiltrating the skeletons with dispersions of the particles and drying the solvent to deposit the particles. On heating, the nanoparticles sinter quickly to strengthen the bonds between the micron-scale skeleton particles and reducing the creep deformations. The particles have been shown to reduce the creep deflections up to 95% and the sintering shrinkage by up to 60%. The maximum benefit is achieved by repeated application of the nanobinder to heal cracks that form when the nanoparticles shrink. Drying the suspension in a magnetic field concentrates the deposits in the interparticle necks where they strengthen the bonds between the particles. Alternatively, the solvent can be dried quickly so that the particle deposits are concentrated near the outer surfaces of the skeleton where the bending stresses are highest. The benefits are highest for parts treated with unoxidized nanoparticles although iron oxide particles also provide a significant benefit. Repeated applications of the nanobinder heal cracks formed by sintering shrinkage and improve the performance of the nanobinder.

The size of the interparticle bonds is increased significantly by nanobinder deposition. However, the increase in bond size is not sufficient to completely explain the reduced creep deformation achieved by nanoparticle treatment. Carbon deposited with the iron nanoparticles is shown to play a critical role in reducing the creep deflection as well, by reducing the self-diffusivity of iron in the alloy. Although the creep deformation can be reduced significantly by simply adding carbon to the skeleton powder, this approach only works when the parts are sintered at high temperature before heating for infiltration. In contrast, nanobinder treatment significantly reduced the creep deformation even without the sintering step. Nanobinder treatment was also more effective than adding carbon alone.

Iron particles were shown to be more effective at creep reduction than iron-oxide particles. However, the difference may be related to the low carbon content of oxide deposits. The performance of oxidized particles might be improved by depositing extra carbon to compensate for reactions with oxygen. Oxidized particles are preferred because they cost less, are not sensitive to air exposure, and may be produced at higher concentrations.

## REFERENCES

- 1 Sachs, E., Cima, M., Williams, P., Brancazio, D., and Cornie, J., "Three Dimensional Printing: Rapid Tooling and Prototypes Directly from a CAD Model", *Journal of Engineering for Industry*, Vol 114, November 1992, p 481-488.
- 2 Sachs, E., Cima, M., Williams, P., Brancazio, D., and Cornie, J., "Three Dimensional Printing Techniques", US Patent # 5,204,055, April 20, 1993.
- 3 Chua, C. K., Leong, K. F., and Lim, C. S., *Rapid Prototyping: Principles and Applications*, World Scientific, 2<sup>nd</sup> Edition, New Jersey, 2003, pp 175,185.
- 4 Allen, S., and Sachs, E., "Three-Dimensional Printing of Metal Parts for Tooling and Other Applications", *Metals and Materials*, Vol 6, No. 6 (2000), pp 589-594.
- 5 Stucker, B., Malhotra, M., Qu, Z., Hardro, P., Mohanty, N., "Rapid Steel Part Accuracy", Solid Freeform Fabrication Symposium, August, 2000.
- 6 Lorenz, A., Sachs, E., Allen, S., Rafflenbeul, L., and Kernan, B., *Metallurgical and Materials Transactions*, 35A, n. 2, 631 (2004).
- 7 Kernan, B., Sachs, E., Allen, S., and Sachs C., "Homogenous Steel Infiltration", SME Technical Paper #TP04PUB219.
- 8 Crane, N. B., "Strengthening Porous Metal Skeletons by Metal Deposition from Nanoparticle Dispersions", PhD Thesis, Massachusetts Institute of Technology, June 2005.
- 9 Domingez, O., and Bigot, J., "Material Transport Mechanisms and Activation Energy in Nanometric Fe Powders Based on Sintering Experiments", *Nanostructured Materials*, vol 6, pp 887-890, 1995.
- 10 Bourell, D. L., and Groza, J. R., "Consolidation of Ultrafine and Nanocrystalline Powder", *ASM Handbook Powder Metal Technologies and Applications*, Vol 7, ASM International, 1998, p 504-515.
- 11 Lekhal, A., Glasser, B. J., and Khinast, J. G., *Chemical Engineering Science*, 56, (2004) p. 4473.
- 12 Vergunst, T., Kapteijn, F., and Moulijn, J. A., *Applied Catalysis A: General*, 213, (2001) p 179.
- 13 Krishtal, M. A., *Diffusion Processes in Iron Alloys*, US Department of commerce, 1970, 0. 91, 103, 129, 139, 177.
- 14 Murray, C. B., Kagan, C. R., and Bawendi, M. G., "Synthesis and Characterization of Monodisperse Nanocrystals and Close-Packed Nanocrystal Assemblies", *Annu. Rev. Mater. Sci.*, 2000, vol 30, p 545-610.